Coastal Engineering 58 (2011) 1072–1088

Contents lists available at ScienceDirect

Coastal Engineering

journal homepage: www.elsevier.com/locate/coastaleng

A two-phase approach to wave-induced sediment transport under sheet flow conditions

Xin Chen [a], Yong Li [b], Xiaojing Niu [a], Daoyi Chen [c], Xiping Yu [a,*]

[a] State Key Laboratory of Hydroscience and Engineering, Department of Hydraulic Engineering, Tsinghua University, Beijing, China
[b] Institute of Mechanics, Chinese Academy of Science, Beijing, China
[c] School of Engineering, University of Liverpool, Liverpool, UK

ARTICLE INFO

Article history:
Received 8 October 2010
Received in revised form 2 May 2011
Accepted 22 June 2011
Available online 18 July 2011

Keywords:
Two-phase flow
Two-fluid model
Oscillatory sheet flow
Sediment transport
Numerical computation

ABSTRACT

A numerical model for the general description of the sediment transport under oscillatory sheet flow conditions is developed based on a two-fluid representation of the two-phase turbulent flows. The governing equations of the model are the Reynolds averaged continuity equations and equations of motion for both the fluid and the sediment phases. The two phases are coupled by the interphase forces including the resistance force, the inertia force, and the lift force. Turbulence closure of the fluid phase is based on a slightly modified k–ε model while an algebraic particle-turbulence model is applied to the sediment phase. The numerical method is based on the modified SIMPLE scheme and an improved time stepping technique. The model is validated by the published data for the symmetrical oscillatory sheet flows generated in an oscillatory flow tunnel at the University of Tokyo and for both the symmetrical and the asymmetrical oscillatory sheet flows generated in an oscillatory flow tunnel at University of Aberdeen. The numerical results on the temporal and spacial variation of the sediment concentration, the horizontal velocities of the two phases, the horizontal and vertical fluxes of the sediment phase, as well as the thickness of the sheet flow layer all show satisfactory agreement with the laboratory data. The model is also shown to predict the net sediment transport rate with a reasonably good accuracy.

1. Introduction

Sediment transport in the sheet flow regime is characterized by a thin layer near the surface of the movable bed with extraordinarily high concentration. Previous studies showed that the sheet flow occurs under wave-induced oscillatory flow conditions when the Shields parameter, an indicator of the movability of the bed materials, becomes larger than a critical value (Horikawa, 1988). It is widely believed that sheet flows play a dominant role in the nearshore topographical change and also in the siltation of navigation channels, particularly during a storm, in such places as Yangtze River estuary and the coastal area along Bohai Bay in China where the seabed is formed by fine sand or silt. Because of the important background in coastal and estuarine engineering, many experimental and numerical studies on oscillatory sheet flows have been carried out and our understanding on the phenomenon has been continuously advancing in the past quarter century. The accumulated knowledge can be found in Horikawa (1988), Fredsoe and Deigaard (1992), Nielsen (1992), Van Rijn (1993).

A significant number of laboratory experiments have been performed to explore the various aspects of the oscillatory sheet flows. The pioneering investigation that has been widely referred in literatures was made by Horikawa et al. (1982) in an oscillatory flow tunnel at the University of Tokyo (UTOFT). The University of Tokyo group continued for quite a long time to investigate the various properties of the sheet flows (Dibajnia and Watanabe, 1992; 1998; Ahmed and Sato, 2003; Watanabe and Sato, 2004). Important earlier contributions were also made by the research group at University of Cambridge (Ahilan and Sleath, 1987; Dick and Sleath, 1992; Zala-Flores and Sleath, 1998). A little later, very detailed data were published by the researchers from Delft Hydraulics or those having the opportunity to use the large oscillatory water tunnel (LOWT) at WL|Delft Hydraulics (Ribberink and Al-Salem, 1995; McLean et al., 2001; Dohmen-Janssen et al., 2001; Dohmen-Janssen and Hanes, 2002; Dohmen-Janssen et al., 2002; Hassan and Ribberink, 2005). The relatively recent contributions are a series of work completed at University of Aberdeen (O'Donoghue and Wright, 2004a, b; Van der et al., 2010), where a large-scale oscillatory flow tunnel (AOFT) equipped with advanced measuring instruments was built in 1999. Other research groups in Japan and in Denmark (Yamashita et al., 1985; Asano, 1995; Li and Sawamoto, 1995; Staub et al., 1996) also carried out experimental studies on the oscillatory sheet flows. Different authors measured the temporal and spacial variation of the sediment concentration, the horizontal and vertical sediment flux, the thickness of the sheet flow layer, etc. under various conditions. In particular, Horikawa et al. (1982) and Yamashita et al. (1985) studied the symmetrical cases assumed to be generated by sinusoidal waves. The asymmetrical cases

* Corresponding author. Tel.: +86 10 62776777.
E-mail address: yuxiping@tsinghua.edu.cn (X. Yu).

0378-3839/$ – see front matter © 2011 Elsevier B.V. All rights reserved.
doi:10.1016/j.coastaleng.2011.06.003

corresponding to the flows induced by cnoidal waves were investigated by Dibajnia (1991), and later on by Ahmed and Sato (2003). Ribberink and Chen (1993), Ribberink and Al-Salem (1994, 1995) and O'Donoghue and Wright (2004a, b) paid attention to the cases with relation to Stokes waves.

In parallel with the experimental studies, efforts have also been made by researchers around the world in the last two decades to develop an advanced numerical model so that the description of the oscillatory sheet flows can be accurate enough. A two-phase model is definitely necessary due to the extraordinarily high concentration of sediment within the sheet flow layer. But the establishment of an effective two-phase flow model is by no means an easily reachable goal and has always been accompanied not only by challenges in understanding the interactions between the two phases and the turbulent features of both the fluid and the sediment phases, but also by difficulties in establishing a refined numerical algorithm that can deal with the complicatedly coupled system of the governing equations for both phases. The earlier work done by Asano (1990) significantly simplified the problem based on the boundary layer approximation and an assumption on the vertical velocity of the sediment phase in addition to the empirical formulas for the turbulent diffusion. Li and Sawamoto (1995) removed the boundary layer approximation in Asano's (1990) model and solved the two dimensional problem straightforwardly. Li and Sawamoto (1995) also tried to improve the empirical expressions for interactions between the fluid and sediments, the interactions among sediment particles, and the turbulent diffusion, but neglected advection effects as well as the diffusion in the horizontal direction. Dong and Zhang (1999), and later on, Liu and Sato (2005; 2006) established an two-phase model of various merits for the oscillatory sheet flows by improving Li and Sawamoto's (1995) work. However, this well established model is still based on the simple mixing-length theory for turbulence closure, and still excludes the advection effects. That the mixing-length coefficient involved in the model is complicatedly related to the features of the flow also restricts its applicability. To enhance the turbulence modeling, Hsu et al. (2003) applied the standard κ–ε model, while Li et al. (2008) employed a one-equation model for simplicity. Bakhtyar et al. (2009a; 2009b) further included the advection effects but unreasonably neglected the diffusion terms in the continuity equations. Longo's (2005) model is a sheet flow model that took into account all the major factors partially considered in the previous models, except for the turbulence modeling of the sediment phase, but it is only for vertically one-dimensional problems. Hsu et al. (2004) and Amoudry et al. (2008) paid attention to the turbulence modeling of the sediment phase. However, Hsu et al. (2004) considered only vertically one-dimensional problems. Amoudry et al.'s (2008) basic equations are multi-dimensional but the solution method is still one-dimensional. In addition, these authors used the concentration-weighted velocities as the variables, so some further manipulations are necessary if the mean velocity of either the sediment phase or the fluid phase is required.

It is worthwhile to mention that the oscillatory sheet flows in practices are usually induced by surface water waves which are not exactly the same as those generated by a horizontal pressure gradient and may have a highly asymmetrical profile. Therefore, to represent the complexity of the oscillatory sheet flows under general conditions, a further enhanced two-phase flow model based on the complete set of governing equations with a thoroughly considered model of turbulence closure and a comprehensive description of the interactions between the two phases, is definitely necessary. The present study is to focus on the development of such a numerical model. We re-derive the basic equations strictly following the standard procedure of Reynolds averaging by considering not only fluctuations of the velocity and the pressure but also the volumetric concentration of the sediment. The interaction forces between the two phases include not only the drag force but also the inertia force and the lift force. Efforts are also made to select the most comprehensive expression for the inter-granular stresses, to find an appropriate algebraic particle-turbulence model for the sediment phase, and to improve the standard k–ε turbulence model for the fluid phase. It is expected that such a model describes not only the sheet flow layer but also the transport of the suspended load and the sediment pick-up/settle-down process. It is also tried to exclude the parts in the existing models that strongly depend on empirical formulas that have very limited validity range. No such a relation that gives the sediment concentration at a particular level or specifies the pick-up rate as a function of the flow parameters will be necessary.

2. Numerical model

2.1. Governing equations

We adopt the two-fluid approach or the Euler–Euler approach. A sediment-fluid two-phase flow can thus be described by the Reynolds averaged continuity equations and equations of motion for both the sediment and the fluid phases. Assuming that the volumetric concentrations of the two phases, the velocities of the two phases, and the pressure can all be decomposed into a mean value and a turbulent fluctuation, and following Elghobashi and Abou-Arab (1983) to model the turbulent correlation terms, we obtain

$$\frac{\partial \alpha_f}{\partial t} + \frac{\partial \alpha_f u_{f,j}}{\partial x_j} = \frac{\partial}{\partial x_j}\left(\frac{\nu_{ft}}{\delta_\alpha}\frac{\partial \alpha_f}{\partial x_j}\right) \tag{1}$$

$$\frac{\partial \alpha_s}{\partial t} + \frac{\partial \alpha_s u_{s,j}}{\partial x_j} = \frac{\partial}{\partial x_j}\left(\frac{\nu_{ft}}{\delta_\alpha}\frac{\partial \alpha_s}{\partial x_j}\right) \tag{2}$$

$$\frac{\partial\left(\alpha_f u_{f,i}\right)}{\partial t} + \frac{\partial\left(\alpha_f u_{f,i} u_{f,j}\right)}{\partial x_j} = -\frac{\alpha_f}{\rho_f}\frac{\partial p}{\partial x_i} + \frac{\partial}{\partial x_j}\left[\alpha_f \nu_f\left(\frac{\partial u_{f,i}}{\partial x_j} + \frac{\partial u_{f,j}}{\partial x_i}\right)\right] + \alpha_f g_i + \frac{\partial}{\partial x_j}\left[\frac{\nu_{ft}}{\delta_\alpha}\left(u_{f,i}\frac{\partial \alpha_f}{\partial x_j} + u_{f,j}\frac{\partial \alpha_f}{\partial x_i}\right)\right] - \frac{F_i}{\rho_f} \tag{3}$$

$$\frac{\partial\left(\alpha_s u_{s,i}\right)}{\partial t} + \frac{\partial\left(\alpha_s u_{s,i} u_{s,j}\right)}{\partial x_j} = -\frac{\alpha_s}{\rho_s}\frac{\partial p}{\partial x_i} + \frac{\partial}{\partial x_j}\left[\alpha_s \nu_s\left(\frac{\partial u_{s,i}}{\partial x_j} + \frac{\partial u_{s,j}}{\partial x_i}\right)\right] + \alpha_s g_i + \frac{\partial}{\partial x_j}\left[\frac{\nu_{ft}}{\delta_\alpha}\left(u_{s,i}\frac{\partial \alpha_s}{\partial x_j} + u_{s,j}\frac{\partial \alpha_s}{\partial x_i}\right)\right] + \frac{F_i}{\rho_s} \tag{4}$$

where, α is the volumetric concentration; u is the velocity; p is the pressure; x is the Cartesian coordinate; t is the time; the subscript f stands for the fluid phase and s stands for the sediment phase; the indices i and j both represent the horizontal and the vertical components and obey the summation convention; ρ is the density; g is the body force; δ_α is the Schmidt number and we assume $\delta_\alpha = 1.0$ in the present study; $\nu_f = \nu_{f0} + \nu_{ft}$ and $\nu_s = \nu_{s0} + \nu_{st}$ are the viscosities of the fluid and the sediment phases, respectively; ν_{ft} and ν_{st} are the turbulent viscosities of the fluid and the sediment phases resulted from turbulence modeling; ν_{f0} is the molecular viscosity of the fluid; ν_{s0} is the viscosity representing the inter-granular stress which can be related to ν_{f0} according to Ahilan and Sleath (1987):

$$\nu_{s0} = \frac{1.2\rho_f}{\rho_s}\left[\left(\frac{\alpha_{sm}}{\alpha_s}\right)^{1/3} - 1\right]^{-2}\nu_{f0} \tag{5}$$

in which, α_{sm} is the maximum volumetric concentration of the sediment phase (it is closely related to the density of the naturally packed sediment and is assumed to be 0.6 in the present study); F_i is the interaction force between the two phases including the drag force, the inertia force, and the lift force in the present study, namely,

$$F_i = F_{d,i} + F_{v,i} + F_{l,i} \tag{6}$$

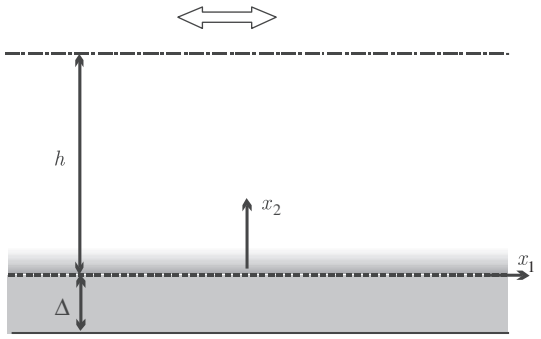

Fig. 1. Definition of domain.

The drag force is given by

$$\mathbf{F}_d = \lambda C_D \frac{3\rho_f \alpha_s}{4D_s}\left|\mathbf{u}_f - \mathbf{u}_s\right|\left(\mathbf{u}_f - \mathbf{u}_s\right) \tag{7}$$

where, the bold face denotes a vector, D_s is the particle diameter of the sediment, C_D is the drag coefficient, and λ is the concentration modification factor. λ may be related to the volumetric concentration of the sediment phase through Tam's (1969) formula while C_D can be expressed as a function of the particle Reynolds number $\mathrm{Re}_s = |\mathbf{u}_f - \mathbf{u}_s| D_s/\nu_{f0}$ through Schiller–Nauman formula (Wörner, 2003):

$$\lambda = \frac{4 + 3\left(8\alpha_s - 3\alpha_s^2\right)^{0.5} + 3\alpha_s}{(2-3\alpha_s)^2} \tag{8}$$

$$C_D = \begin{cases} \dfrac{24}{Re_s}\left(1.0 + 0.15Re_s^{0.687}\right) & (Re_s \le 1000) \\ 0.44 & (Re_s > 1000) \end{cases} \tag{9}$$

The inertia force and the lift force are formulated as

$$\mathbf{F}_v = C_M \rho_f \alpha_s \frac{d\left(\mathbf{u}_f - \mathbf{u}_s\right)}{dt} \tag{10}$$

$$\mathbf{F}_l = C_L \rho_f \alpha_s \left(\mathbf{u}_f - \mathbf{u}_s\right) \times \Omega \tag{11}$$

where Ω is the vorticity vector of the fluid phase, $C_M = 0.5$ is the added-mass coefficient and $C_L = 0.5$ is the lift coefficient.

It is worthwhile to point out that the right hand side of Eqs. (1) and (2) as well as the next to the last terms in Eqs. (3) and (4) originate from modeling the correlation product of the fluctuations of the volume concentration and the velocity components, and represent the effects of sediment diffusion. We should also note that $\alpha_f + \alpha_s = 1$.

2.2. Turbulence model

The turbulence model selected for the fluid phase in the present study is essentially the k–ε model, i.e., the turbulent viscosity of the fluid phase is given by

$$\nu_{ft} = C_\mu \frac{k_f^2}{\varepsilon_f} \tag{12}$$

where C_μ is a constant, k is the turbulent kinetic energy, and ε is the turbulent kinetic energy dissipation rate. Following Elghobashi and Abou-Arab's (1983) approach while paying attention to the compatibility with the standard k–ε model, we can derive the following governing equations for k and ε:

$$\frac{\partial\left(\alpha_f k_f\right)}{\partial t} + \frac{\partial\left(\alpha_f k_f u_{fj}\right)}{\partial x_j} = \frac{\partial}{\partial x_j}\left(\alpha_f \nu_{fk}\frac{\partial k_f}{\partial x_j}\right) + \alpha_f\left(G_f - \varepsilon_f\right) \tag{13}$$

$$\frac{\partial\left(\alpha_f \varepsilon_f\right)}{\partial t} + \frac{\partial\left(\alpha_f \varepsilon_f u_{fj}\right)}{\partial x_j} = \frac{\partial}{\partial x_j}\left(\alpha_f \nu_{f\varepsilon}\frac{\partial \varepsilon_f}{\partial x_j}\right) + \frac{\alpha_f}{k_f}\left(C_1 G_f \varepsilon_f - C_2 \varepsilon_f^2\right) \tag{14}$$

where $\nu_{fk} = \nu_{ft}/\delta_k$, $\nu_{f\varepsilon} = \nu_{ft}/\delta_\varepsilon$, $\delta_k = 1.0$, $\delta_\varepsilon = 1.33$, $C_1 = 1.44$, $C_2 = 1.92$, and G_f stands for

$$G_f = \nu_{ft}\frac{\partial u_{f,i}}{\partial x_j}\left(\frac{\partial u_{f,i}}{\partial x_j} + \frac{\partial u_{f,j}}{\partial x_i}\right) \tag{15}$$

The turbulent viscosity of the sediment phase is assumed to follow Hinze–Tchen's (Hinze, 1975) law, i.e.,

$$\nu_{st} = \left(1 + \frac{\tau_s}{\tau_f}\right)^{-1}\nu_{ft} \tag{16}$$

$$\tau_f = 1.22 C_\mu^{0.75}\frac{k_f}{\varepsilon_f} \tag{17}$$

$$\tau_s = \frac{\rho_s D_s^2}{18\rho_f \nu_{f0}\left(1 + 0.15Re_s^{0.687}\right)} \tag{18}$$

where τ_f is the turbulence time scale of the fluid phase and τ_s is the response time of the sediment phase. Note that Hinze–Tchen's algebraic particle-turbulence model is a simple but standard model for two-phase flows. Its validity conditions may be referred to Johnson (1998) and these conditions are essentially to require that the size of the sediment particle be small.

It is worthwhile to point out that there is no study that has justified the accuracy of the standard k–ε model even for the fluid phase in a sediment-laden flow of very high concentration. Turbulence modeling of the sheet flows, which are characterized by their high sediment

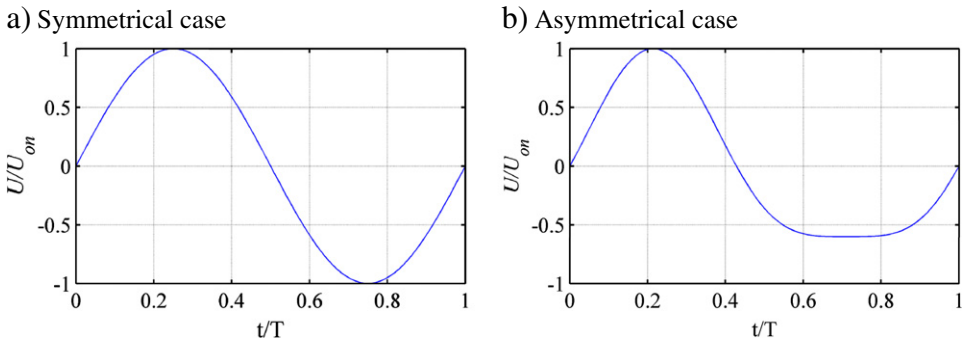

Fig. 2. Velocity profile of the outer flow.

Table 1
Experimental conditions of the symmetrical sheet flow cases.

Test case	U_0 (m/s)	D_s (mm)	ρ_s (kg/m^3)	T (s)
AOFT-LS612	1.26	0.13	2650	6.0
UTOFT-HWK	1.27	0.2	2660	3.6

concentration, is thus an unsolved problem. In practice, Katori et al. (1996) adopted the one-equation (k-equation) model with an empirical formula for the turbulence energy dissipation rate, while Li et al. (2008) applied the same one-equation model but required the turbulent viscosity and the dissipation to take different values in low and high concentration regions. Two-equation turbulence models adopted by Elghobashi and Abou-Arab (1983) and Hsu et al. (2003) did not consider the effects of the sediment concentration. In the present study, we apply the k–ε model but allow a modification of C_μ in Eq. (12) from its standard value of 0.09. C_μ in the present study is assumed to be a function of the sediment concentration as follows

$$C_\mu = 0.09\left(1-\frac{\alpha_s}{\alpha_m}\right)^n \tag{19}$$

where $n=5$ is taken in the present study by calibration. Eq. (19) is essentially empirical, but it allows a smooth transition from the pore flow within the sandy bottom to the dilute flow. The former can be reasonably assumed to be laminar, while the latter may be described by the standard k–ε model. The most distinguished advantage of introducing Eq. (19) is that the two-phase turbulent flow model reasonably covers the whole range of sediment concentration and needs no empirical relation that gives the sediment concentration at a particular level or specifies the pick-up rate as a function of the flow parameters when applied to describe sediment transport over a sandy bed. It is worthwhile to point out that the importance to consider the

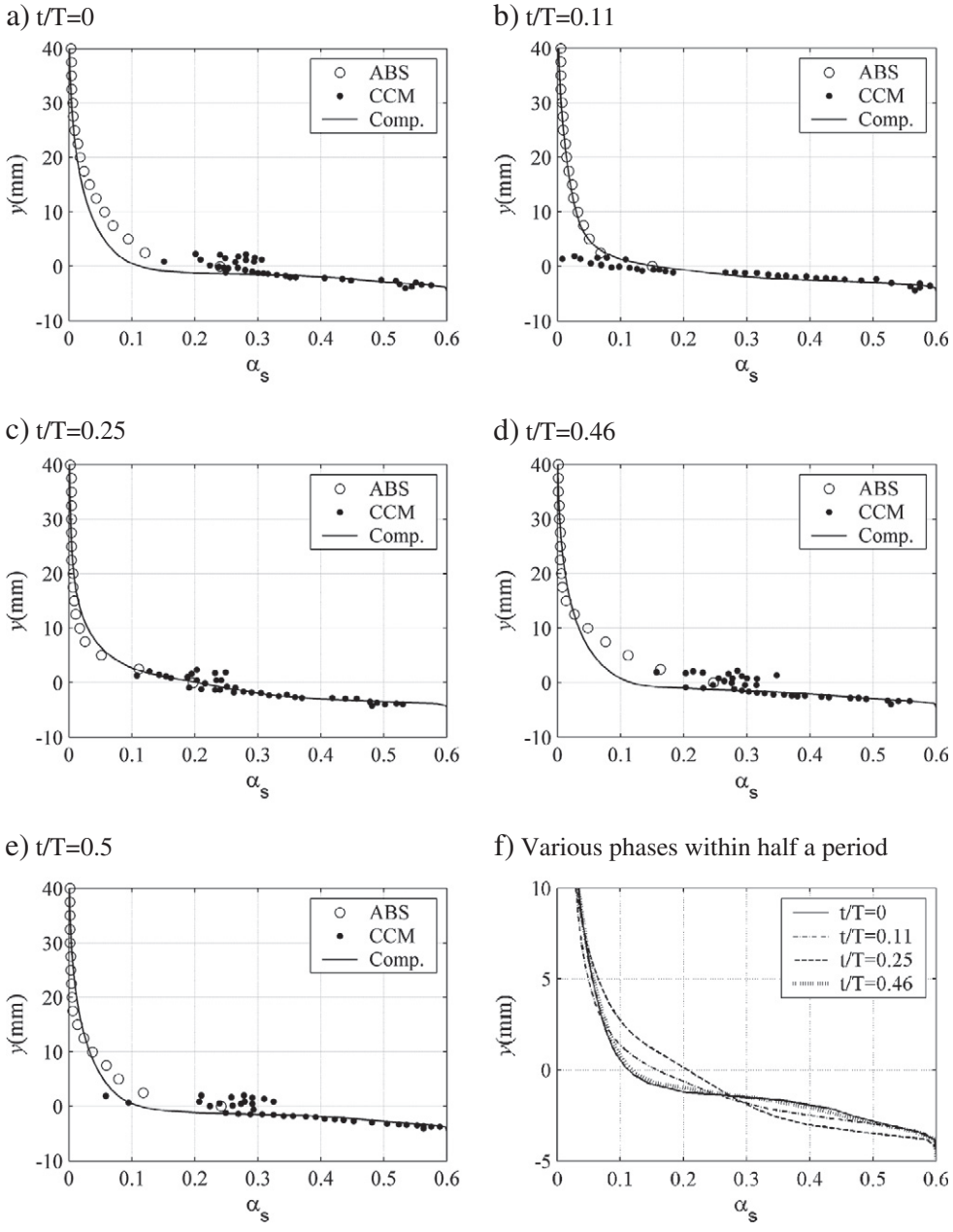

Fig. 3. Sediment concentration at different phases (Case AOFT-LS612).

dependence of the turbulence intensity on the sediment concentration has already been realized in a number of previous studies. Li et al. (2008) introduced a concentration-weighted formula for the turbulent viscosity in their one-equation (k-equation) model, which decreases with the increase of the sediment concentration; Liu and Sato (2005, 2006) adopted a varying function of the vertical coordinate as their expression of the eddy viscosity; Dong and Zhang (2002) considered the dependence of the vertical diffusion coefficient on the sediment concentration. Amoudry et al. (2008) employed a similar relation as Eq. (19). Because the sheet flow is characterized by a small thickness with the turbulent viscosity at both the upper and lower edges being given, Eq. (19), with a properly chosen value should be a reasonable approximation in modeling sheet flows. In this study, we tried different values of n and found that the erosion depth is in best agreement with the measurement when $n=5$. It may be worthwhile to emphasize that the generality of $n=5$ should not be overestimated.

2.3. Boundary and initial conditions

For model verification, we restrict our interest to the sheet flow induced by an oscillatory flow driven by horizontal pressure gradient as shown in Fig. 1. When the sand bed under the still water condition, i.e., the bed formed as all the suspended sediments settle down, is taken as the reference level, our domain is considered to vary from $y=-\Delta$ to $y=h$, where h is the thickness of the fluid flow which is affected by the sheet flow, and Δ is the thickness of the moving sediment layer. In practice, Δ can be a relatively large constant so that the whole moving sediment layer is included. For simplicity, the top boundary at $y=h$ is assumed to be a 'rigid-lid'. The boundary conditions then require the sediment flux and the gradient of all other variables, including $u_{f,1}$, $u_{f,2}$, $u_{s,1}$, $u_{s,2}$, k_f and ε_f, to vanish in the vertical direction. Vanishment of the sediment flux means

$$\kappa_s \frac{\partial \alpha_s}{\partial x_2} - u_{s,2}\alpha_s = 0 \tag{20}$$

At the bottom boundary $y=-\Delta$, non-slip condition is assumed. Hence, $u_{f,1}$, $u_{f,2}$, $u_{s,1}$, $u_{s,2}$, k_f and ε_f all equal to zero. The sediment concentration, however, should be given by

$$\alpha_s = \alpha_{sm} \tag{21}$$

Since the flow is driven by a horizontal pressure gradient, the two lateral boundary conditions should satisfy

$$\frac{\partial p}{\partial x_1} = -\rho_f \frac{dU}{dt} \tag{22}$$

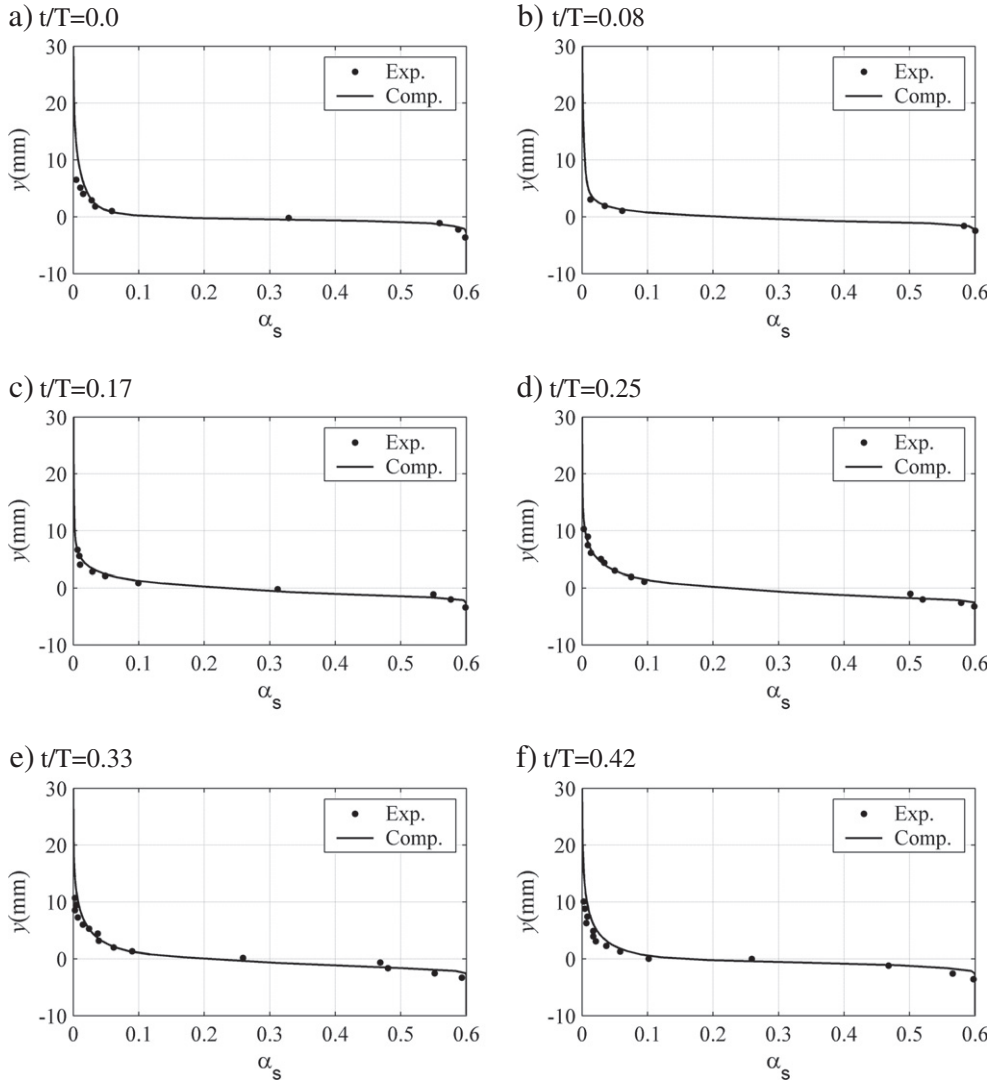

Fig. 4. Sediment concentration at different phases (Case UTOFT-HWK).

in which,

$$U = \begin{cases} U_0 \cos\omega t & [\textit{corresponding to small amplitude wave}] \\ U_1 \cos\omega t + U_2 \cos 2\omega t & [\textit{corresponding to second order Stokes wave}] \end{cases} \quad (23)$$

where, if the pressure gradient is physically considered as caused by the oscillatory outer flow of a boundary layer, U_0 corresponds to the amplitude of the outer flow induced by a linear wave; U_1 and U_2 are the amplitudes of the first and second harmonic components of the outer flow induced by a 2nd-order Stokes wave; ω is the oscillatory frequency. In addition, the horizontal gradient of all other variables, includingα_s, $u_{f,1}$, $u_{f,2}$, $u_{s,1}$, $u_{s,2}$, k_f and ε_f, must equal to zero.

The still water condition is assumed to be the initial condition. Thus, at $t=0$, all flow variables are zero, while $\alpha_s=0$ at $y>0$ and $\alpha_s=\alpha_{sm}$ at $y<0$.

2.4. Numerical method

The modified SIMPLE scheme of Patankar (1980) is employed to solve the basic Eqs. (1)–(4) as well as the k and ε Eqs. (13) and (14). These differential equations are therefore discretized over a staggered rectangular grid, based on the finite volume method. The convection terms are treated following the third order QUICK scheme of Tao (2001), and the diffusion terms treated following the second order central difference scheme. A modified TDMA scheme is used to solve the sparse difference equations.

The time stepping strategy is standard. At each time step, the volumetric concentration of each phase is computed first. Then, the velocities of each phase are predicted and a modification of the pressure is made. The values of the velocities can therefore be updated to satisfy the conservation laws for the mass and momentum. If necessary, modification of the pressure and the velocity can be repeated to yield converged values being used as the initial conditions of the next step. The convergence is judged by the residuals of volume flux in the pressure modification equation. Once the volumetric concentration and the velocity of each phase are determined, the turbulence kinetic energy and the turbulence kinetic energy dissipation rate can be readily obtained. When the relative difference of the sediment concentration and the velocity of each phase between two adjacent cycles are lesser than a prescribed level (it is specified to be

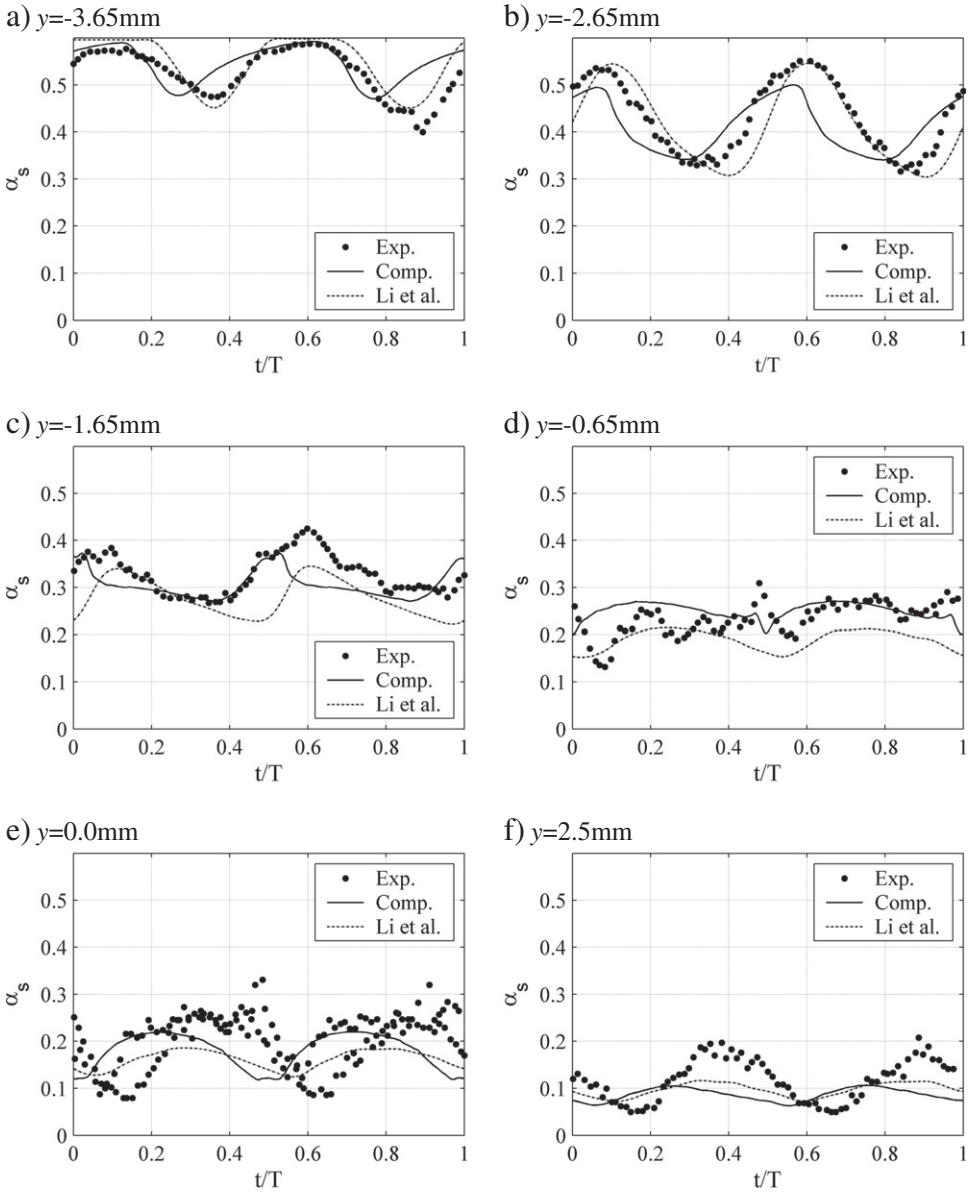

Fig. 5. Sediment concentration at different elevations (Case AOFT-LS612).

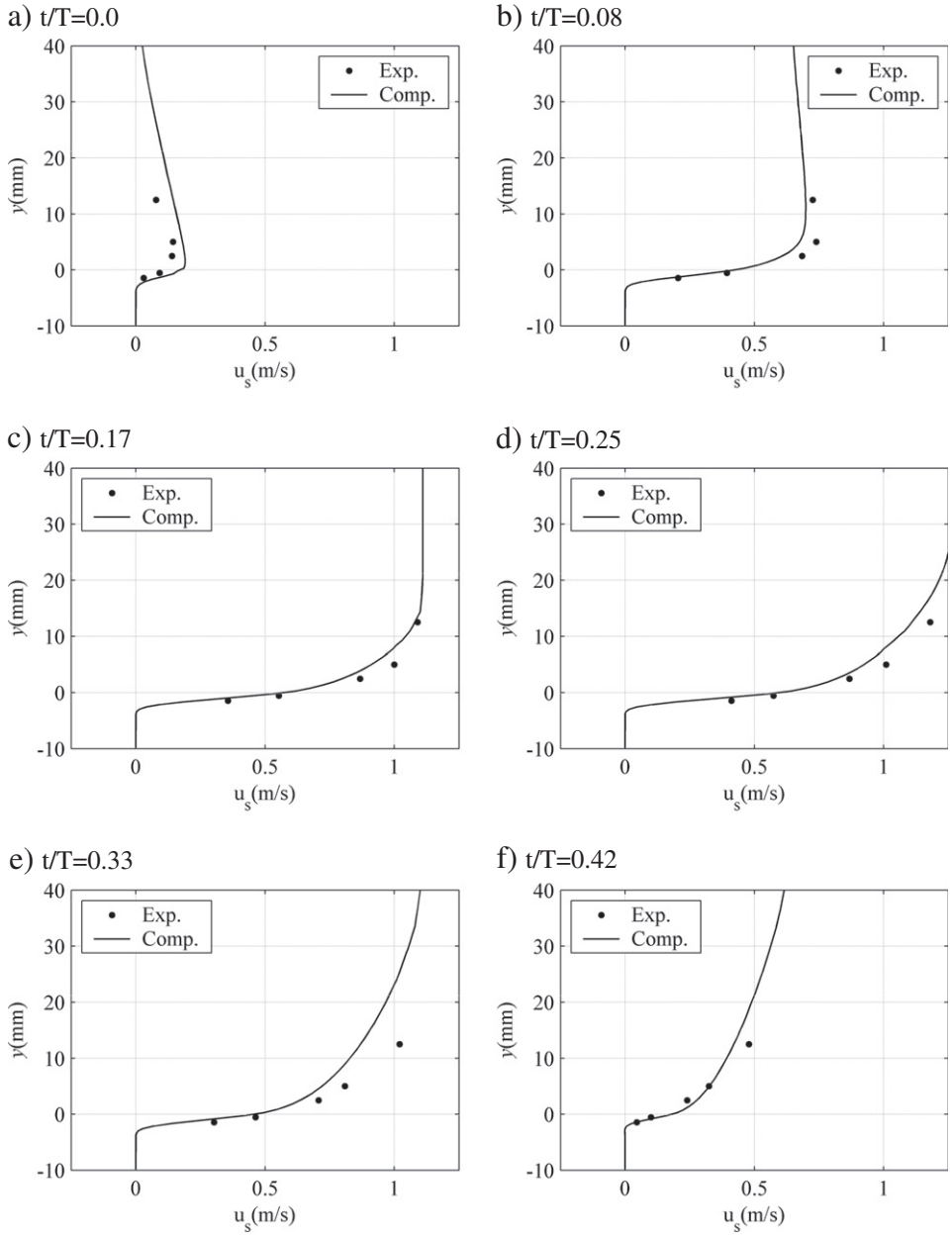

Fig. 6. Horizontal velocity of sediment phase at different phases (Case AOFT-LS612).

10^{-4} in the following studies), the computation is terminated, and the solution of the last cycle represents the oscillatory sheet flow under consideration.

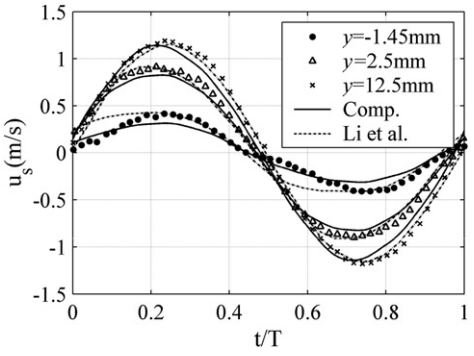

Fig. 7. Horizontal velocity of sediment phase at different levels (Case AOFT-LS612).

3. Results and discussions

The model established in the present study is to be validated by carefully measured data in the oscillatory flow tunnel at the University of Tokyo (UTOFT) and in the oscillatory flow tunnel at University of Aberdeen (AOFT). The UTOFT experiments were carried out by Horikawa et al. (1982) with median-sized sediment ($d_{50}=0.2$ mm) on symmetrical oscillatory sheet flows. The AOFT experiments were carried out by O'Donoghue and Wright (2004a, b) and Li et al. (2008) with various sediment size [$d_{50}=0.13$ mm (fine)/0.27 mm (median)/0.46 mm (coarse)] on both symmetrical and asymmetrical oscillatory sheet flows. The temporal profiles of the outer flows that induce the sheet flows of our interest are shown in Fig. 2. The asymmetry parameter of the oscillatory outer flow is defined as

$$a = \frac{U_{on}}{U_{on} + U_{off}} \tag{24}$$

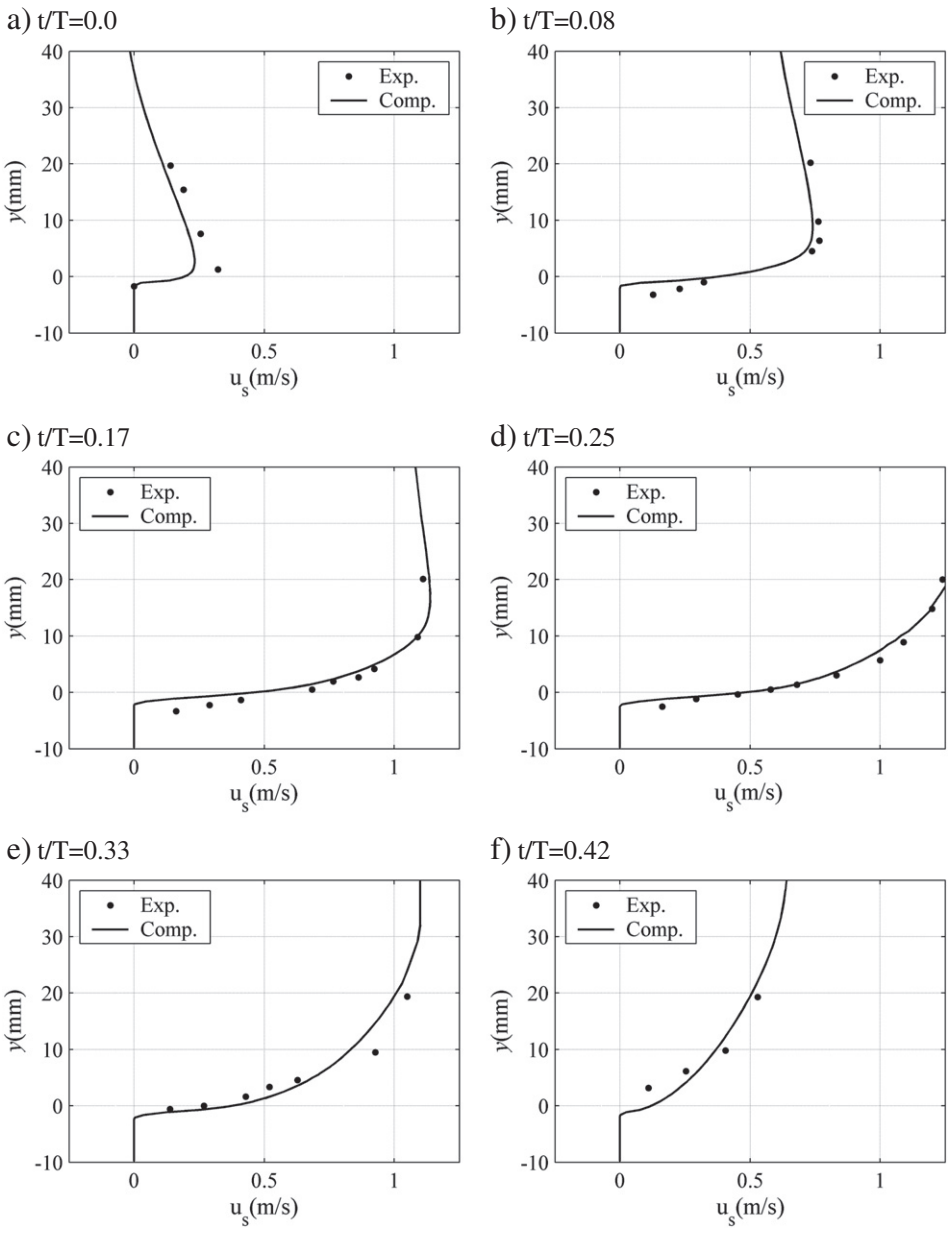

Fig. 8. Horizontal velocity of sediment phase at different phases (Case UTOFT-HWK).

where U_{on} and U_{off} represent the maximum velocities in the onshore (positive x) and offshore (negative x) directions, respectively. $a=1/2$ correspond to the symmetrical case. In the numerical computations, the domain in the vertical direction is fixed by $h=5$cm and $\Delta=2$cm. The horizontal grid size is set to be 10 mm while the vertical grid size is equivalent to the median sediment size (0.2 mm) near the bottom and increases proportionally to about 2 mm at the surface.

3.1. Symmetrical sheet flows

The fine sediment case of the AOFT experiments (Case AOFT-LS612) and the median sediment case of the UTOFT experiments (Case UTOFT-HWK) are adopted in this study to represent the sediment motion under symmetrical sheet flow conditions. Table 1 summarizes the experimental conditions.

Fig. 3 shows the computed and measured distributions of the volumetric concentration of sediment in Case AOFT-LS612 at different onshore phases. Because the flow is symmetrical, we need only to show the results in half a period. The experimental data were obtained with an Acoustic Back Scatting system (ABS) in the relatively low concentration region and a Conductivity Concentration Meter (CCM) in the relatively high concentration region. At all phases, the numerical results are shown to agree very well with the experimental

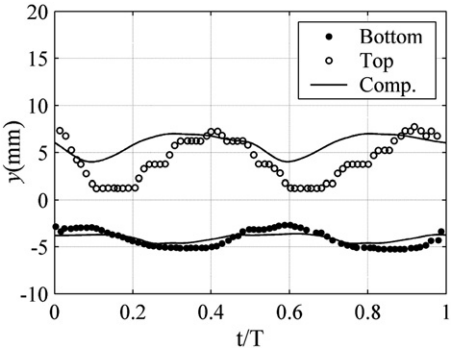

Fig. 9. The sheet flow layer (Case AOFT-LS612).

data below the reference level at $y=0$, but some discrepancies are observed at $y>0$. It is not easy to conclude whether the errors are due to the computation or the measurement, but the experimental data do have some inconsistency. Firstly, ABS and CCM give quite different results nearby the reference level. Secondly, integrations of the concentration profile above and below the reference level are different (particularly at $t=0$, $t/T=0.46$, $t/T=0.5$), which is against the mass conservation law for the sediment. Finally, some measured values of the sediment concentration become less than zero (for example, at $t/T=0.11$), which is physically impossible. When all computed concentration profiles at different phases are plotted together, as shown in Fig. 3(f), it seems that the profiles at different phases have a pivot where the volumetric concentration is nearly invariant and a pivoting motion of the profile can be observed as the phase varies. The elevation of the pivot is below the reference level, and the averaged volumetric concentration at the pivot is about 0.26–0.27 (about 0.44 times of the maximum value), which confirms the conclusion of O'Donoghue and Wright (2004a). It is also evident that, during a period of the oscillation, both the volumetric concentration and the scour depth increase as the velocity of the driven flow increases, and they reach their maximums at about $t/T=0.25$ corresponding to the maximum velocity of the driven flow, as shown in Fig. 3(f).

Fig. 4 shows the numerical and experimental results on the volumetric concentration of sediment in Case UTOFT-HWK at different onshore phases. The computed results agree with the measured data at each phase even better than in Case AOFT-LS612, especially at the region above the reference level. Again, a pivot of the concentration profiles, with a vertical position below the reference level and a nearly invariant volumetric concentration of about 0.26–0.27, can be observed.

Fig. 5 compares the computational and experimental results of the sediment concentration in Case AOFT-LS612 at several different elevations near the reference level. It is shown that, at $y=-3.65$ mm, both the computed and measured concentrations vary from nearly the maximum value (0.6) to a value in between of 0.5 and 0.4. This level should then be rather close to the lower boundary of the sheet flow layer. The peak duration of the concentration profile is significantly longer than the trough duration at this level. This is not difficult to understand considering that the initial motion of a sediment particle

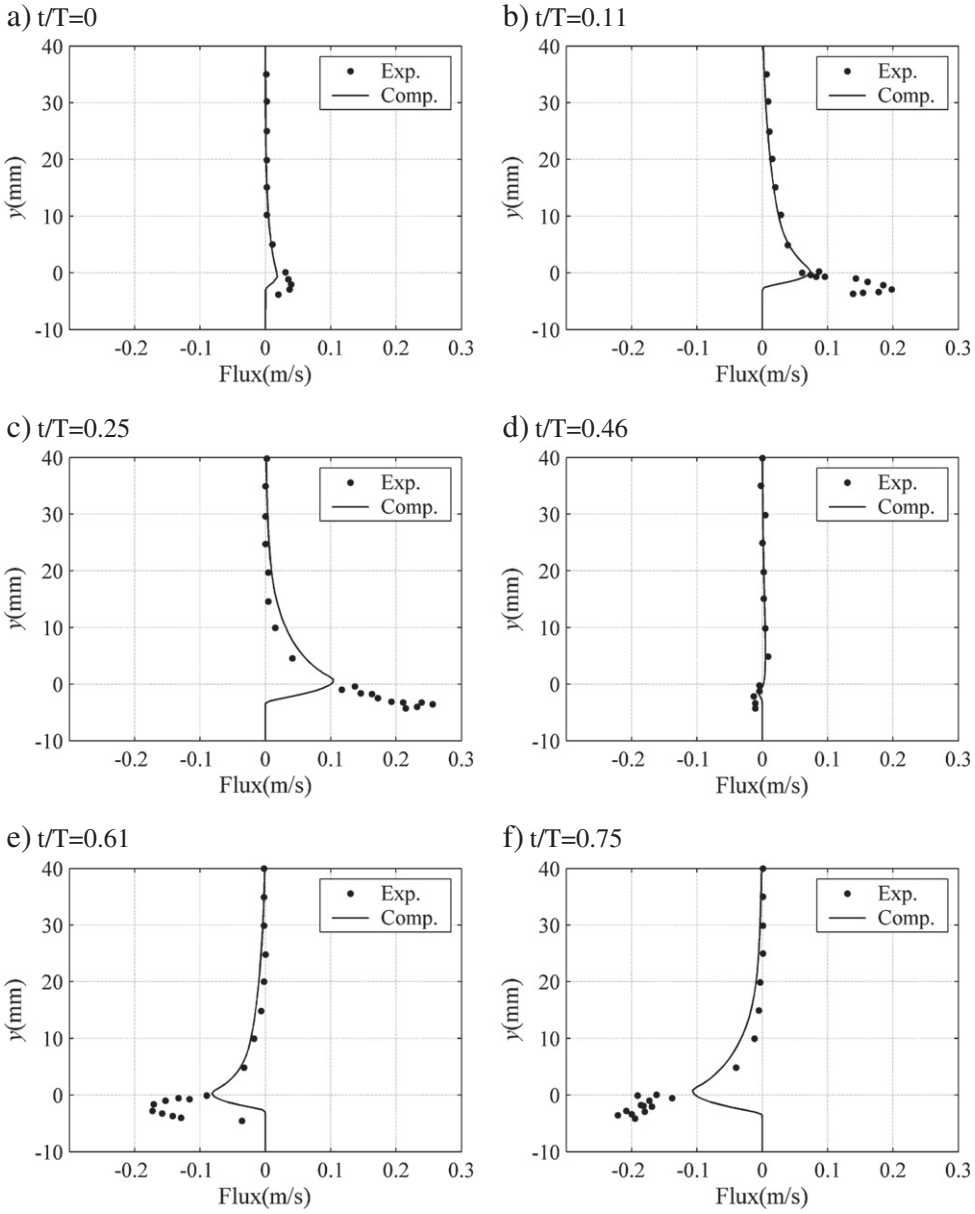

Fig. 10. Horizontal volumetric flux of sediment at different phases (Case-LS612).

must break its threshold. It is also clear that the peak duration has a tendency to decrease while the trough duration increase as the level of interest increases. They become comparable at y = −2.65 mm. At y = −1.65 mm, the peak duration becomes evidently shorter and the trough duration longer. The level corresponding to y = −0.65 mm is rather close to the pivot of the concentration profile, so the variation of the concentration with time is mild. At y = 0, the computation and the experiment are in rather good agreement if we pay no attention to the phase lag. The reason for causing the phase lag is difficult to be identified, because the pick-up and the settle-down of sediment particles at this level are both of very high rates, neither the computation nor the measurement can be done with very good accuracy. In fact, the experimental data by CCM and ABS are quite different. It should also be pointed out that the difference between the numerical and the experimental results above the reference level seems to be larger as compared to those below the reference level, particularly in the region with relatively low concentration. This is probably because the turbulence model we used for densed two-phase flows is not accurate enough. For comparison, Li et al. (2008) computational results are also plotted in Fig. 5. The present model does not seem to have evidently improved the accuracy of prediction, but this does not damage the advantage of the present model because it avoided quite a number of empirical formulas employed in Li et al.'s (2008) model.

Fig. 6 is a comparison of the computed horizontal velocity of the sediment phase with that measured in Case AOFT-LS612 at different onshore phases. It is noted that the computed results agree with the measured data very well. There is no experimental data at y>0.03 m because the sediment concentration in this region is at a very low level and the velocity of the sediment phase becomes very close to the velocity of the fluid. Fig. 7 compares the computed horizontal velocity of the sediment phase with that measured in Case AOFT-LS612 and numerical results of Li et al. (2008) at different levels. The agreement of the computed results from both the present model and Li et al.'s (2008) model with the measured data is also very good.

Fig. 8 compares the computed horizontal velocity of the sediment phase with that measured in Case UTOFT-HWK at different phases. The agreement between the computational and the experimental results is also very satisfactory. Slightly different from what is shown in Fig. 6, the numerical results at t = 0 in this case underestimate the

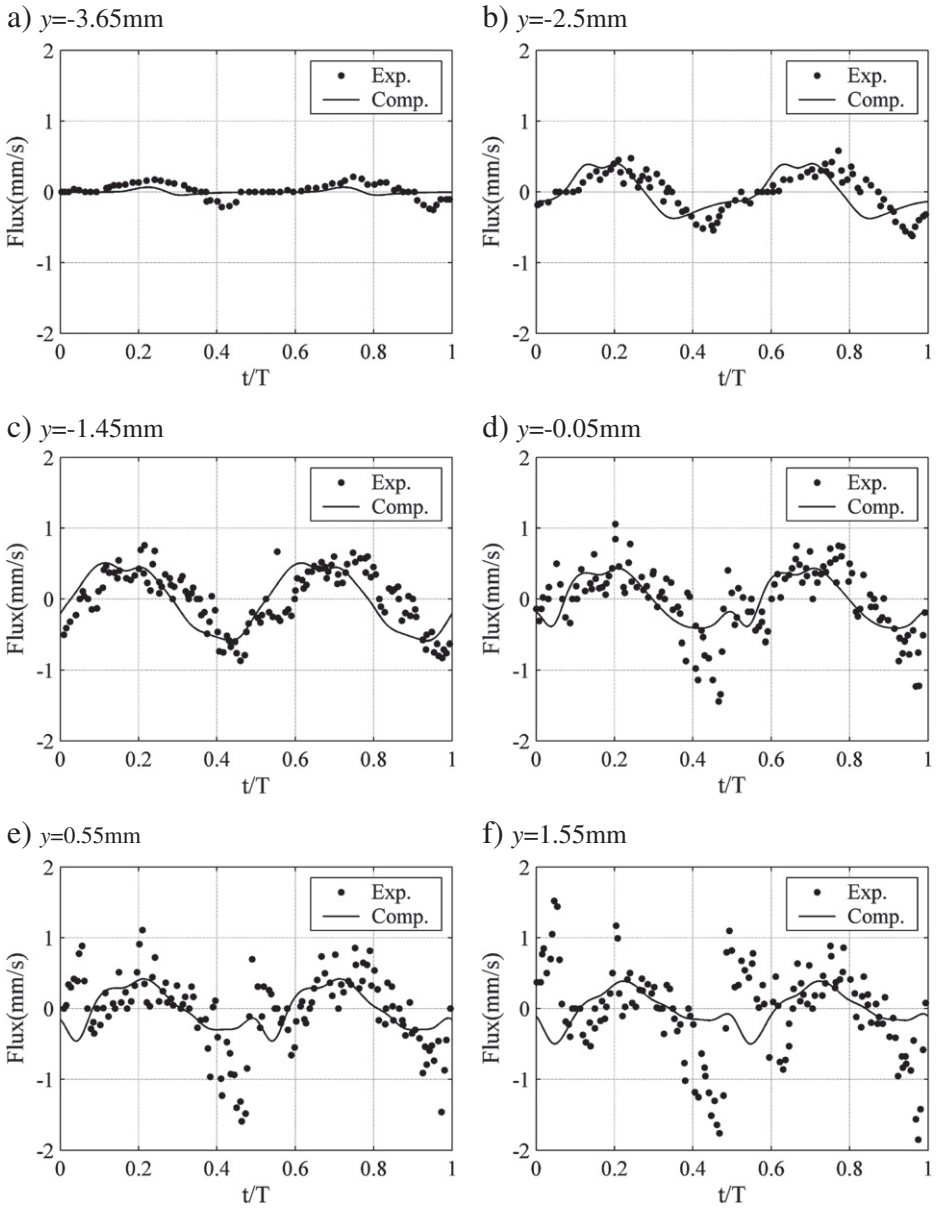

Fig. 11. Vertical volumetric flux of sediment at different levels (Case-LS612).

Table 2
Experimental conditions of the asymmetrical sheet flow cases.

Test case	U_1 (m/s)	U_2 (m/s)	a	D_s (mm)	T (s)	q_s (mm^2/s)
AOFT-FA5010	1.2	0.3	0.63	0.13	5.0	−128.0
AOFT-MA5010	1.2	0.3	0.63	0.27	5.0	52.6
AOFT-CA5010	1.2	0.3	0.63	0.46	5.0	44.1
AOFT-FA7515	1.2	0.3	0.63	0.13	7.5	−88.3
AOFT-MA7515	1.2	0.3	0.63	0.27	7.5	35.9
AOFT-CA7515	1.2	0.3	0.63	0.46	7.5	33.8
AOFT-LA612	1.2	0.3	0.63	0.13	6.0	−61.0
AOFT-LA406	1.0	0.25	0.63	0.13	4.0	−8.0

q_s is the measured net sediment transport rate.

measurements, rather than overestimate as in Case AOFT-LS612. This is probably an effect of the sediment size when the driving flow reverses its direction.

Fig. 9 shows the computed and the measured variation of the sheet flow layer within a period in Case AOFT-LS612. The upper and lower boundaries of the layer are defined at the positions where the sediment concentration equals to 0.05 and 0.99α_{sm}, respectively. The agreement between the computation and the experiment is acceptable. Both the numerical and the experimental results show that the upper boundary of the sheet flow layer approaches its peak shortly after the lower boundary of the sheet flow layer reaches its trough, and the upper boundary gets to its trough shortly after the lower boundary reaches its peak. This is a direct consequence of the physical process that the sediments on the bed are picked up and transported vertically as the driving flow is accelerated while the suspended sediments settle down and deposit on the bed as the driving flow is decelerated.

Fig. 10 shows the horizontal volumetric flux of sediment at different phases in Case AOFT-LS612. The computational and experimental results show almost the same tendency of variation within a period, both being in phase with the velocity of the fluid

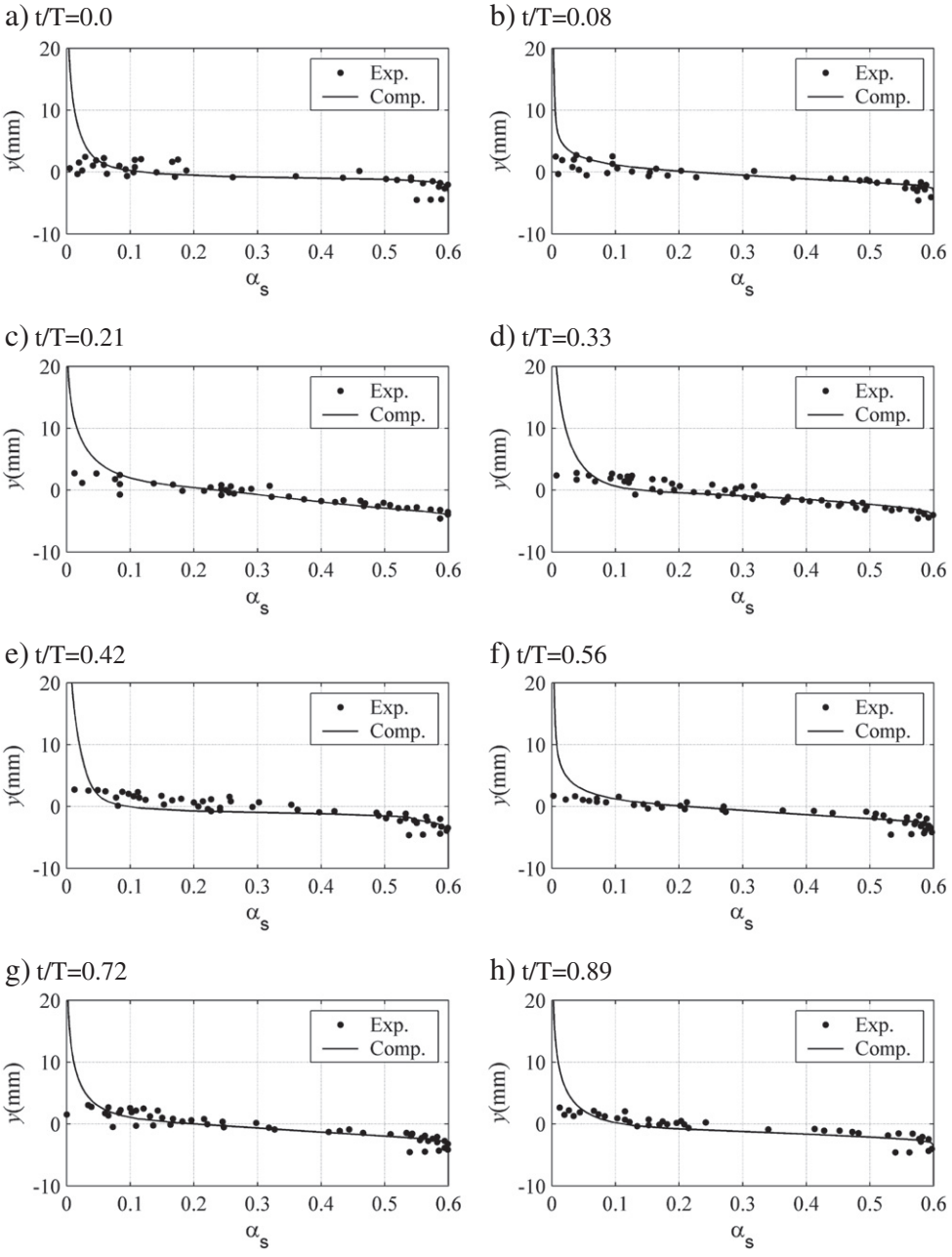

Fig. 12. Sediment concentration at different phases (Case AOFT-MA5010).

phase and sharply reaching a maximum near the reference level, but they differ significantly by magnitude, particularly near the reference level. It may be necessary to point out that to obtain a good agreement between the computations and the experiments near the reference level is a very big challenge because both the numerical model and the experimental method cannot be as good as they are in other regions.

Fig. 11 shows the computed and measured vertical volumetric flux of sediment at different levels in Case AOFT-LS612. The agreement between the computations and measurements is fairly good, particularly in the region below the reference level, although the measured data is rather scattered. Study on the vertical flux of sediment is important because it is actually the net sediment pick-up rate (Nielsen et al., 2002; Li et al., 2008), or the difference between the pick-up rate and the deposition rate, a concept critical to the sediment transport model dealing only the suspended load. It is evident in Fig. 11 that the vertical flux of sediment increases as the driving flow

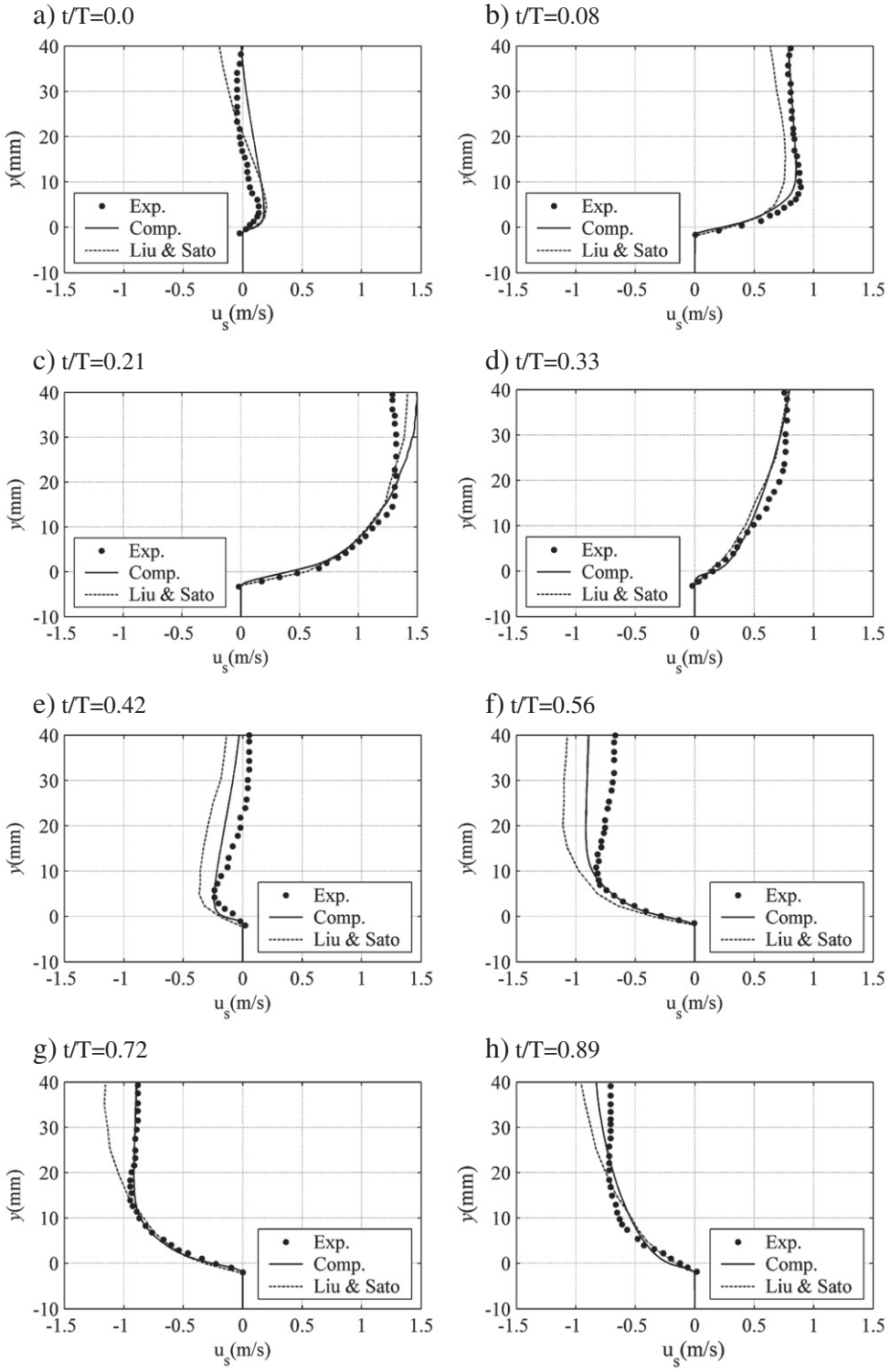

Fig. 13. Horizontal velocity of sediment phase at different phases (Case AOFT-MA5010).

is accelerated and decreases as the driving flow is decelerated. The maximum rate appears when the horizontal velocity of the fluid phase reaches its maximum, and the minimum rate appears when the fluid flow reverses its direction. It should also be noted that the magnitude of the net sediment pick-up rate varies with the elevation. This implies that when an empirical function on pick-up rate is to be established, a relevant elevation at which the function is valid should first be specified.

3.2. Asymmetrical sheet flows

O'Donoghue and Wright (2004a, b) and Li et al.'s (2008) experiments, all done in AOFT, are used to represent the asymmetrical sheet flows in this study. Table 2 lists the parameters of the experimental cases cited in this section. Case numbering follows the original authors. Among all the cases given in Table 2, Case AOF-MA5010 is used to verify the geometric, kinematics, and dynamic features of the sheet flow layer. A different case (Case AOFT-LA612), which yields to a negative net sediment transport rate, is used to verify the flux of the sediment transport because the existing empirical models usually fails to represent an offshore net transport case. All cases are referred when the net sediment transport rate is studied.

Fig. 12 shows the computed and measured volumetric concentration of sediment at different phases in Case AOFT-MA5010. The computational results agree well with the experimental data except in the region above the reference level. The accuracy of the experiment in the region above the reference level does not seem to be good enough because there are even some negative values. As in the symmetrical cases, existence of a pivot of the concentration profile can still be observed at a position below the reference level and the value of volumetric concentration there is almost invariant and equal to about 0.3.

Fig. 13 compares the computed horizontal velocity of the sediment phase with that measured in Case AOFT-MA5010 at different phases. For comparison, Liu and Sato's (2006) numerical results are also shown. The computed results of the present model agree well with the experimental data in general. But, the agreement in the upper region is obviously not as good as in the fine sediment cases of AOFT-LS612 and UTOFT-HWK under symmetrical flow conditions, as shown in Figs. 6 and 8. The reason is probably related to the loss of accuracy of the turbulence model in some extent when the sediment size becomes large. It is demonstrated that the present model gives better results of horizontal velocity of the sediment phase than Liu and Sato's (2006) even the erosion depth and the bed level in their model must be determined empirically.

Fig. 14 shows the computed and the measured horizontal velocity of the sediment phase at three different elevations in Case AOFT-MA5010. Agreement between the computations and the measurements is very good. Determined by the asymmetry of the horizontal velocity of the driving flow, the temporal variation of the horizontal velocity of the sediment phase is also asymmetrical. In addition, the ratio of the peak to trough values varies with the elevation. At $y=-2$ mm, there is only onshore sediment transport, or, the sediment particles move only when t/T is in between of 0.10 and 0.35. At $y=0$ mm, the ratio of the peak to trough values of the horizontal velocity of the sediment phase is about 2 and this value is decreased to about 1.5 at $y=5$ mm. Onshore and offshore durations of the horizontal velocity of the sediment phase seem to rely on the asymmetry of the driving flow velocity and do not vary with the elevation.

Fig. 15 shows the computed and measured variation of the sheet flow layer within a period in Case AOFT-MA5010. The agreement between the computations and experiments is again very good. The maximum thickness of the sheet flow layer, corresponding to both the deepest scouring and the highest uplifting of sediment, occurs shortly after the peak of the driving flow. Governed by the driving flow, the peak induced sheet flow has a much larger thickness than the trough induced one, but has a shorter duration.

Fig. 16 presents the computed and measured horizontal volumetric flux of sediment at different phases in Case AOFT-LA612. The agreement between the computations and the measurements is reasonably good. The vertical distribution of the flux at each phase is shown to have a maximum near the reference level. The sediment flux is in the onshore direction from $t/T=0$ to some instant in between of $t/T=0.32$–0.42, and in the offshore direction from some instant in between of $t/T=0.32$–0.42 and $t/T=1$.

Fig. 17 presents the computed and measured vertical volumetric flux of sediment or the net pick-up rate at six elevations in Case AOFT-LA612. The experimental data below zero show a clear tendency but those above zero are rather scattered. Similar to the symmetrical case, the net pick-up rate is closely related to the velocity of the driving flow. It is evident that the pick-up rate has two peaks within a period, a large peak corresponding to the peak of the driving flow and a small peak corresponding to the trough of the driving flow. The pick-up rate also shows some correlation with the horizontal flux of sediment. When the horizontal flux increases, the pick-up rate takes a relatively large value.

Fig. 18 compares the computed net sediment transport rate with experimental data, together with frequently used empirical formulas of, Dibajnia and Watanabe (1996), Dibajnia et al. (2001), and numerical results of Liu and Sato (2006). Experimental data corresponding to different sediment diameters are distinguished by different marks in the figures. The computed results of the present model show the best agreement with the experimental data both in terms of direction and of magnitude, and the relative error is within 50% [Fig. 18(d)]. As it can be realized from the measured values given in Table 2, the net sediment transport rate of the 8 cases concerned in

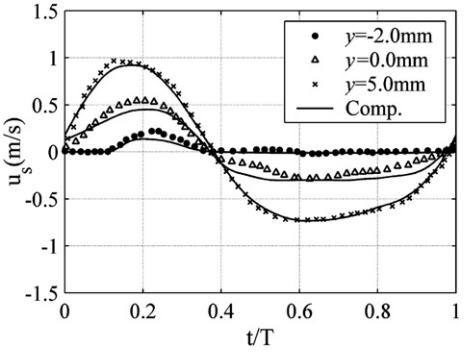

Fig. 14. Horizontal velocity of sediment phase at different elevations (Case AOFT-MA5010).

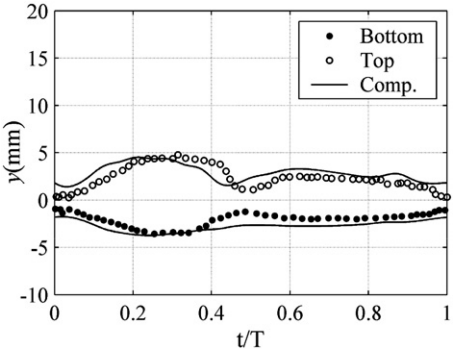

Fig. 15. The sheet flow layer (Case AOFT-MA5010).

the present comparison is actually very complicatedly related to the sediment diameter, the period of the oscillation, the amplitude of the velocity of the driving flow, etc., and it takes negative values (offshore drift) for fine sediment and positive values (onshore drift) for the median and coarse sediments. The empirical formulas failed to describe the offshore drift of sediment in some extent, as demonstrated in Fig. 18(a, b), but the present numerical model works. The agreement of the numerical results of Liu and Sato's (2006) with

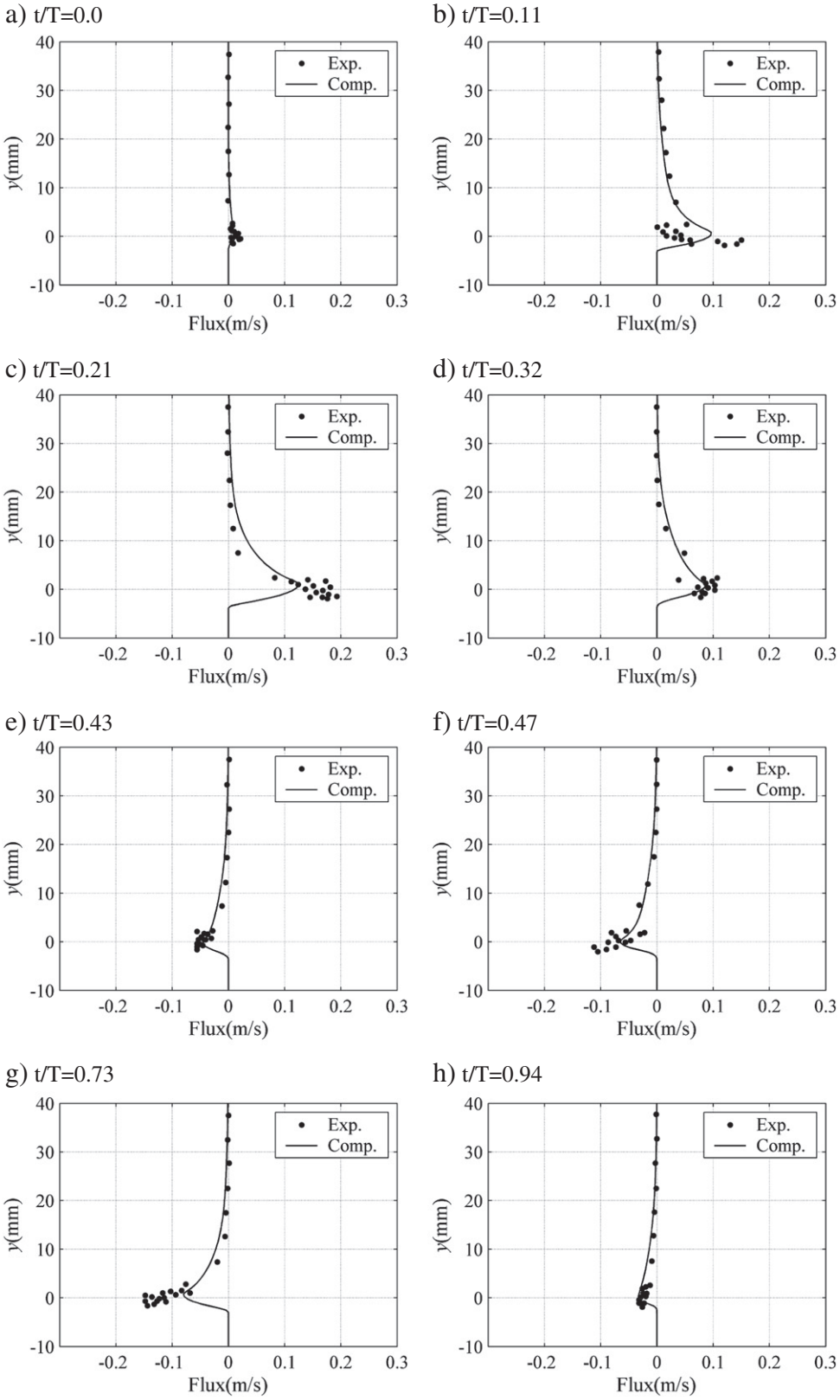

Fig. 16. Horizontal volumetric flux of sediment at different phases (Case AOFT-LA612).

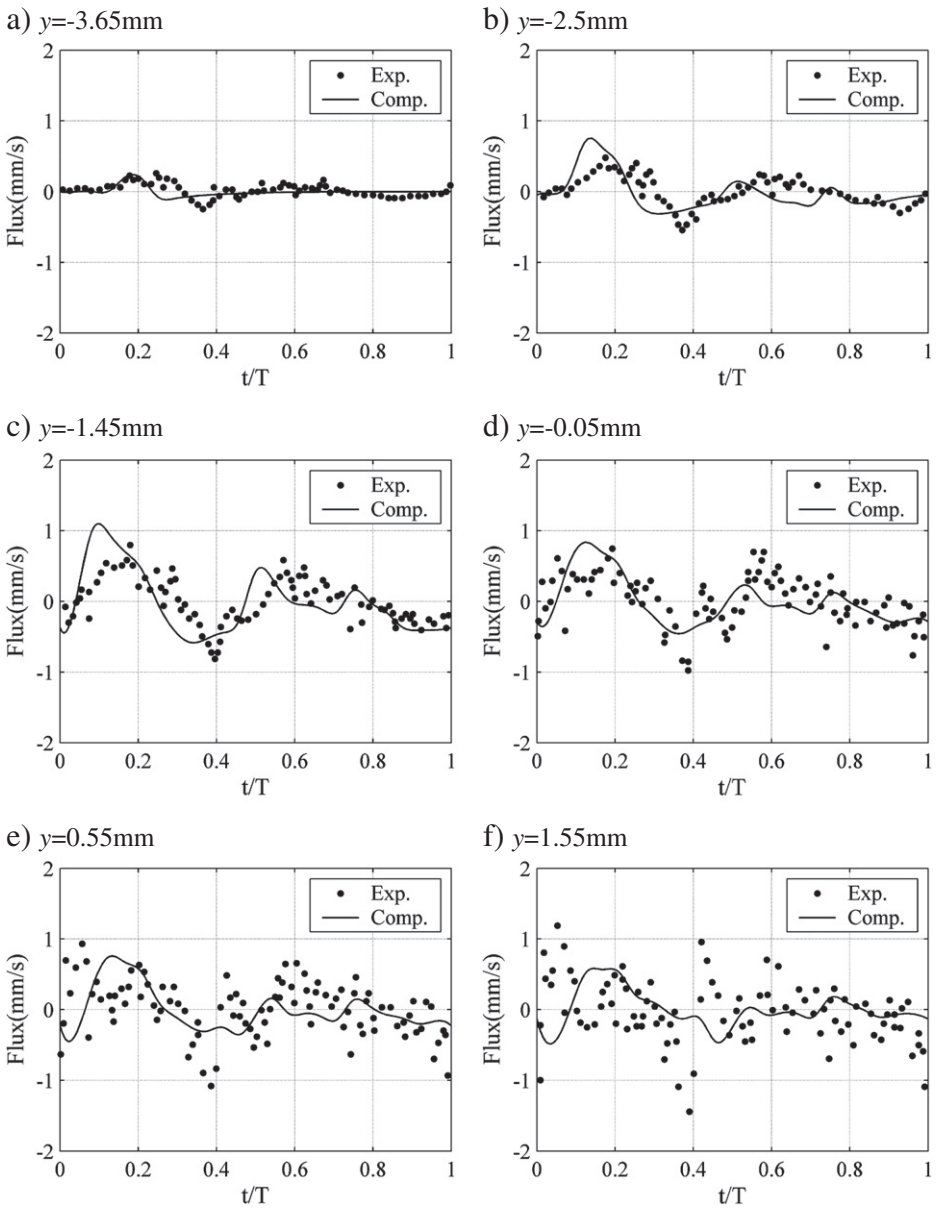

Fig. 17. Vertical volumetric flux of sediment at different levels (Case AOFT-LA612).

experimental data does not show any advantage of their model over the present one even it employed empirical formulas to determine the erosion depth and the bed level.

4. Conclusions

A numerical model based on the direct solution of the Euler–Euler formulation of two-phase flows is proposed to describe the sediment-laden flows under sheet flow conditions. The fluid phase and the sediment phase in the model are coupled through the interaction forces between the two phases including the drag force, the inertia force, and the lift force. Since the model is expected to be valid within a wide range from the critically incepted granular layer, in which inter-granular stresses play dominant roles, to the dilute region where the turbulence is important, efforts are made to select the most comprehensive expression for inter-granular stresses, to find an appropriate algebraic particle-turbulence model for the sediment phase, and to improve the standard k–ε turbulence model for the fluid phase. Modification of the conventional expressions for the interphase forces is also carried out so as to include the effects of sediment concentration. The model is validated by carefully measured data about fine/median/coarse sediment in an oscillatory flow tunnel at the University of Tokyo (UTOFT) and in the oscillatory flow tunnel at University of Aberdeen (AOFT). The UTOFT experiments were carried out on symmetrical oscillatory sheet flows. The AOFT experiments were carried out on both symmetrical and asymmetrical oscillatory sheet flows. The computed results on the temporal and spacial variation of the sediment concentration, the horizontal velocities of the two phases, the horizontal and vertical fluxes of the sediment, as well as the thickness of the sheet flow layer under both symmetrical and asymmetrical cases all show satisfactory agreement with the measured data. The model can also accurately predict the net sediment transport rate, which is very complicatedly related to the sediment diameter, the period of the oscillation, the amplitude of the velocity of the driving flow, etc., and takes negative values in some cases and positive values in other cases, while most of the empirical formulas fail to describe the offshore drift of sediment.

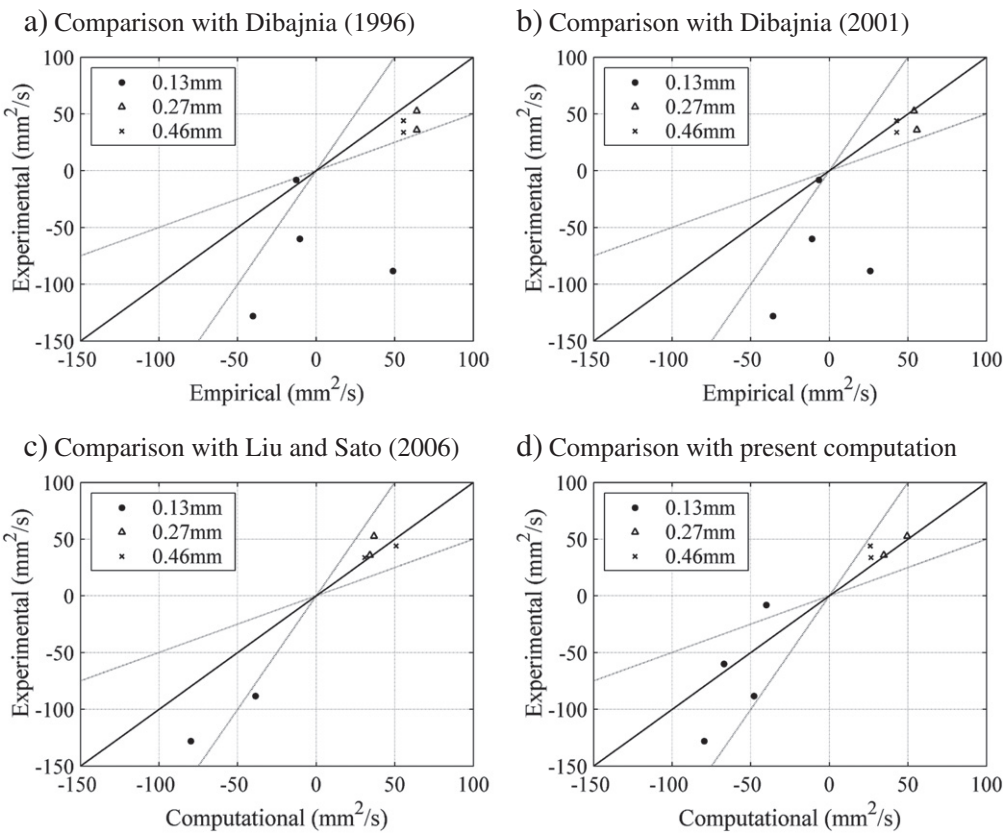

Fig. 18. Comparison of net sediment transport rates.

Acknowledgments

This work is partially supported by Natural Science Foundation of China (NSFC) under grant No. 10772099 and by State Key Laboratory of Hydroscience and Engineering under grant No. 2011-KY-1. The first author also thanks China Scholarship Council (CSC) for providing him an opportunity to visit School of Engineering, University of Liverpool, UK for one year, and he would also like to thank Dr. Ming Li at University of Liverpool for his kind help.

Appendix

Notations

a	asymmetry parameter
C_μ	turbulence model constant
C_1	turbulence model constant
C_2	turbulence model constant
C_D	drag force coefficient
C_L	lift force coefficient
C_M	add-mass force coefficient
D_s	sediment diameter
f	fluid phase
$F_{d,i}$	drag force
$F_{k,i}$	force between phases
$F_{v,i}$	added-mass force
$F_{l,i}$	lift force
$g_{k,i}$	body force
G_f	turbulence generating term
h	thickness of the fluid flow
i,j	directions in horizontal and vertical
p	pressure
q_s	measured net sediment transport rate
Re_s	particle Reynolds number
s	sediment phase
T	period of oscillatory flow
t	time
U_{on}	maximum velocities of onshore
U_{off}	maximum velocities of offshore
U	free stream velocity
U_0	basic component of sinusoidal waves
U_1	first harmonic components of 2nd-order Stokes waves
U_2	second harmonic components of 2nd-order Stokes waves
$u_{k,i}$	phase velocity
x_j	Cartesian coordinate
y	distance to the zero elevation
α_k	volumetric concentration
α_{sm}	maximum volumetric concentration, 0.6 is used in present study
λ	concentration modification factor for drag force
Δ	the thickness of the moving sediment layer
δ	Schmidt number
δ_k	turbulence model constant
δ_ε	turbulence model constant
ν_f	fluid viscosity coefficient
ν_f	sediment viscosity coefficient
ν_{f0}	fluid kinetic viscosity coefficient
ν_{ft}	fluid turbulent viscosity coefficient
ν_{s0}	inter-granular stress viscosity coefficient
ν_{st}	sediment turbulent viscosity coefficient
ρ	phase density
τ_f	turbulence time scale of fluid phase
τ_s	response time of sediment phase
ω	frequency of oscillatory flow

References

Ahilan, R.V., Sleath, J., 1987. Sediment transport in oscillatory flow over flat beds. Journal of Hydraulic Engineering 113, 308–322.

Ahmed, A.S.M., Sato, S., 2003. A sheet flow transport model for asymmetric oscillatory flows part I: uniform grain size sediments. Coastal Engineering Journal 45 (3), 321–337.

Amoudry, L., Hsu, T.-J., Liu, P.L.-F., 2008. Two-phase model for sand transport in sheet flow regime. Journal of Geophysical Research 113, C03011. doi:10.1029/2007JC004179.

Asano, T., 1990. Two-phase flow model on oscillatory sheet-flow. Proceedings, 22nd International Conference on Coastal Engineering. ASCE, pp. 2372–2384.

Asano, T., 1995. Sediment transport under sheet-flow conditions. Journal of Water, Port, Coast, and Ocean Engineering 121 (5), 239–246.

Bakhtyar, R., Yeganeh-Bakhtiary, A., Barry, D.A., Ghaheri, A., 2009a. Two-phase hydrodynamic and sediment transport modeling of wave-generated sheet flow. Advances in Water Resources 32, 1267–1283.

Bakhtyar, R., Yeganeh-Bakhtiary, A., Barry, D.A., Ghaheri, A., 2009b. Euler–Euler coupled two-phase flow modeling of sheet flow sediment motion in the nearshore. Journal of Coastal Research 56, 467–474.

Dibajnia, M., 1991. Study on Nonlinear Effects in Beach Processes. PhD thesis, University of Tokyo.

Dibajnia, M., Moriya, T., Watanabe, A., 2001. A representative wave model for estimation of near shore local transport rate. Coastal Engineering in Japan 43 (1), 138.

Dibajnia, M., Watanabe, A., 1992. Sheet flow under non linear waves and currents. Proceedings, 23rd International Conference on Coastal Engineering. ASCE, pp. 2015–2028.

Dibajnia, M., Watanabe, A., 1996. A transport rate formula for mixed-sized sands. Proceedings, 25th International Conference on Coastal Engineering. ASCE, pp. 3791–3804.

Dibajnia, M., Watanabe, A., 1998. Transport rate under irregular sheet flow conditions. Coastal Engineering 35, 167–183.

Dick, J., Sleath, J., 1992. Sediment transport in oscillatory sheet flow. Journal of Geophysical Research 97 (C4), 5745–5758.

Dohmen-Janssen, C.M., Hanssan, W.N., Ribberink, J.S., 2001. Mobile-bed effects in oscillatory sheet flow. Journal of Geophysical Research 106 (C11), 103–115.

Dohmen-Janssen, C.M., Hanes, D.M., 2002. Sheet flow dynamics under monochromatic nonbreaking waves. Journal of Geophysical Research 107 (C10), 3149.

Dohmen-Janssen, C.M., Kroekenstoel, D.F., Hassan, W.N., Ribberink, J.S., 2002. Phase lags in oscillatory sheet flow: experiments and bed load modelling. Coastal Engineering 46, 61–87.

Dong, P., Zhang, K., 1999. Two-phase flow modeling of sediment motions in oscillatory sheet flow. Coastal Engineering 36, 87–109.

Dong, P., Zhang, K., 2002. Intense near-bed sediment motions in waves and currents. Coastal Engineering 45, 75–87.

Elghobashi, S.E., Abou-Arab, T.W., 1983. A two-equation turbulence model for two-phase flows. Physics of Fluids 26, 931–938.

Fredsoe, J., Deigaard, R., 1992. Mechanics of Coastal Sediment Transport. World Scientific, Singapore.

Hassan, W.N., Ribberink, J.S., 2005. Transport processes of uniform and mixed sands in oscillatory sheet flow. Coastal Engineering 52, 745–770.

Hinze, J.O., 1975. Turbulence. McGraw-Hill, New York.

Horikawa, K., 1988. Nearshore Dynamics and Coastal Processes. University of Tokyo Press, Tokyo.

Horikawa, K., Watanabe, A., Katori, S., 1982. Sediment transport under sheet flow condition. Proceedings, 18the International Conference on Coastal Engineering. ASCE, pp. 1335–1352.

Hsu, T., Chang, H., Hsieh, C., 2003. A two-phase flow model of wave-induced sheet flow. Journal of Hydraulic Research 41 (3), 299–310.

Hsu, T., Jenkins, J.T., Liu, P., 2004. On two-phase sediment transport: sheet flow of massive particles. Proceedings of the Royal Society of London A460, 2223–2250.

Johnson, R.W., 1998. The Handbook of Fluid Dynamics. CRC Press.

Katori, S., Mizuguchi, M., Watanabe, A., 1996. A numerical model of sheet flow sediment transport. Proceedings, 25th International Conference on Coastal Engineering 1996. ASCE, pp. 3818–3829.

Li, M., Pan, S., O'Connor, B.A., 2008. A two-phase numerical model for sediment transport prediction under oscillatory sheet flows. Coastal Engineering 55, 1159–1173.

Li, L., Sawamoto, M., 1995. Multi-phase model on sediment transport in sheet-flow regime under oscillatory flow. Coastal Engineering in Japan 38 (2), 157–178.

Liu, H., Sato, S., 2005. Modeling sediment movement under sheet flow conditions using a two-phase flow approach. Coastal Engineering Journal 47 (4), 255–284.

Liu, H., Sato, S., 2006. A two-phase flow model for asymmetric sheet flow conditions. Coastal Engineering 53, 825–843.

Longo, S., 2005. Two-phase flow modeling of sediment motion in sheet-flows above plane beds. Journal of Hydraulic Engineering 131 (5), 366–379.

McLean, S.R., Ribberink, J.S., Dohmen-Janssen, C.M., Hassan, W.N., 2001. Sand transport in oscillatory sheet flow with mean current. Journal of Waterway, Port, Coastal, and Ocean Engineering 127 (3), 141–151.

Nielsen, P., 1992. Coastal Bottom Boundary Layers and Sediment Transport. World Scientific, Singapore.

Nielsen, P., vander Wal, K., Gillan, K., 2002. Vertical fluxes of sediment in oscillatory sheet flow. Coastal Engineering 45, 61–68.

O'Donoghue, T., Wright, S., 2004a. Concentrations in oscillatory sheet flow for well sorted and graded sands. Coastal Engineering 50, 117–138.

O'Donoghue, T., Wright, S., 2004b. Flow tunnel measurements of velocities and sand flux in oscillatory sheet flow for well-sorted and graded sands. Coastal Engineering 51, 1163–1184.

Patankar, S.V., 1980. Numerical Heat Transfer and Fluid Flow. Hemispher Publishing Corporation.

Ribberink, J.S., Al-Salem, A.A., 1994. Sediment transport in oscillatory boundary layers in cases of rippled beds and sheet flow. Journal of Geophysical Research 99 (C6), 12707–12727.

Ribberink, J.S., Al-Salem, A.A., 1995. Sheet flow and suspension of sand in oscillatory boundary layers. Coastal Engineering 25, 205–225.

Ribberink, J.S., Chen, Z., 1993. Sediment Transport of Fine Sand under Asymmetric Oscillatory Flow. Report H840, Part VII. Delft Hydraulics, The Netherlands.

Staub, C., Jonsson, I.G., Svendsen, I.A., 1996. Sediment suspension in oscillatory flow: measurements of instantaneous concentration at high shear. Coastal Engineering 27, 67–96.

Tam, C.K.W., 1969. The drag on a cloud of spherical particles in low Reynolds number flow. Journal of Fluid Mechanics 38, 537–546.

Tao, W., 2001. Numerical Heat Transfer. Xi'an Jiaotong University Press, Xian. (in Chinese).

Van der, A,.D.A., O'Donoghue, T., Ribberink, J.S., 2010. Measurements of sheet flow transport in acceleration-skewed oscillatory flow and comparison with practical formulations. Coastal Engineering 57, 331–342.

Van Rijn, L.C., 1993. Principles of sediment transport in rivers. Estuaries and Coastal Seas. Aqua Publications, Amsterdam.

Watanabe, A., Sato, S., 2004. A sheet-flow transport rate formula for asymmetric forward-leaning waves and currents. Proceedings, 29th International Conference on Coastal Engineering, pp. 1703–1714.

Wörner, M., 2003. A compact introduction to the numerical modeling of multiphase flows. Forschungszentrum Karlsruhe GmbH. Karlsruhe, Germany.

Yamashita, T., Sawamoto, M., Takeda, H., Yokomori, G., 1985. A study on oscillatory flow and sediment transport at sheet-flow condition. Proceedings, Japanese Conference on Coastal Engineering. JSCE, pp. 297–301 (in Japanese).

Zala-Flores, N., Sleath, J., 1998. Mobile layer in oscillatory sheet flow. Journal of Geophysical Research 103 (C6), 12,783–12,793.